Available online at www.sciencedirect.com
SCIENCE DIRECT®
Global and Planetary Change 38 (2003) 209–222
GLOBAL AND PLANETARY CHANGE
www.elsevier.com/locate/gloplacha

Development of the minimal advanced treatments of surface interaction and runoff

Kumiko Takata[a,*], Seita Emori[a,1], Tsutomu Watanabe[b]

[a] *Frontier Research System for Global Change, Showa-machi, Kanazawa-ku, Yokohama 236-0001, Japan*
[b] *Forestry and Forest Products Research Institute, Tsukuba, Ibaraki 305-8687, Japan*

Received 24 November 2001; received in revised form 2 April 2002; accepted 27 May 2002

Abstract

A land surface model (LSM), minimal advanced treatments of surface interaction and runoff (MATSIRO), has been developed for climate studies at the global and regional scales. The canopy has a single layer, whose albedo and bulk coefficients are evaluated on the basis of a multilayer canopy model. The fluxes are calculated from the energy balance at the ground and canopy surfaces in snow-free and snow-covered portions considering the subgrid snow distribution. The interception evaporation from canopy and the transpiration on the basis of photosynthesis are treated. A simplified TOPMODEL is used to calculate runoff. The snow has the variable number of layers from one to three in accordance with snow water equivalent (SWE), and the snow temperature is calculated by a thermal conduction equation. Besides, the snowmelt, the refreeze of snowmelt, and the freeze of rainfall in snow are taken into consideration. It is found in the PILPS 2e experiment that some parameters in the runoff scheme, such as the surface hydraulic conductivity and the river channel fraction, have a considerable impact on the partitioning of the surface runoff and the base flow. The snow albedo is prognosticated from the time passage since last snowfall and the snow temperature. The soil has five layers in this version, and the soil temperature, the soil moisture, and the frozen amount of moisture are calculated.

Keywords: Double-source model; TOPMODEL; Land surface model; GCM

1. Introduction

A number of land surface models (hereafter LSMs) have been developed to be used in global or regional climate models (e.g., Sellers et al., 1996; Dickinson et al., 1998). These models incorporate the radiation transfer, the evaporation, the transpiration, the snow, the runoff, and so on considering the effects of vegetation, and solve the energy and water exchange between land and atmosphere as the vertical one-dimensional processes. The minimal advanced treatments of surface interaction and runoff (MATSIRO) has been developed to be coupled with the atmospheric general circulation model developed at the Center for Climate System Research, the University of Tokyo, and the National Institute for Environmental Studies, CCSR/NIES AGCM (Numaguti et al., 1997). That is projected to be used in climate studies at the

* Corresponding author. Tel.: +81-45-778-5700; fax: +81-45-778-5706.
E-mail address: takata@jamstec.go.jp (K. Takata).
[1] On leave from the National Institute for Environmental Studies, Onogawa, Tsukuba 305-8506, Japan.

0921-8181/03/$ - see front matter © 2003 Published by Elsevier Science B.V.
doi:10.1016/S0921-8181(03)00030-4

time scales from a month to a few centuries, and at the resolutions larger than tens of kilometers. MATSIRO is intended to represent all the important processes for the water and energy exchange between land and atmosphere, at that time and spatial scales, in a physically based way, i.e., *advanced*, though in a simple manner, i.e., *minimal*.

MATSIRO has been developed on the basis of the land surface scheme of CCSR/NIES AGCM (Numaguti et al., 1997). In CCSR/NIES AGCM, a bucket-type hydrology model and a single-layer snow scheme are adopted. With a single-layer snow model, the predicted snow surface temperature tends to be inaccurate when snow mass is high, thus the snow scheme has been modified to a multilayer model. Since the snow albedo has considerable impacts on the land surface processes and hence on the atmosphere, a prognostic snow albedo scheme has been implemented. The effect of canopy is considered in a rather simple way in the bucket-type model in CCSR/NIES AGCM; that is, the albedo and the roughness are prescribed in accordance with the vegetation type. In MATSIRO, they have been parameterized based on a multilayer canopy model after Watanabe (1994). As for runoff, there is only the saturation excess runoff in the bucket-type model. However, the horizontal heterogeneity of soil moisture caused by the topography has a significant effect on runoff (e.g., Famiglietti and Wood, 1994; Stieglitz et al., 1997; Koster et al., 2000; Warrach et al., 2002). The simplified TOPMODEL (Beven and Kirkby, 1979) has been adopted for runoff in MATSIRO so that the surface runoff and the base flow are estimated separately. The stomatal resistance is prescribed at a constant rate in the bucket-type model. That was calculated from an empirical equation (Jarvis-type model) in the first version of MATSIRO (Takata and Emori, 1999), and has been recently replaced by a photosynthetic scheme on the basis of physiology (Farquhar-type model) after SiB2 (Sellers et al., 1996). The Farquhar-type model is used as a de facto standard in LSMs, owing to the progress in studies of the interaction between climate and the terrestrial ecosystem. In this

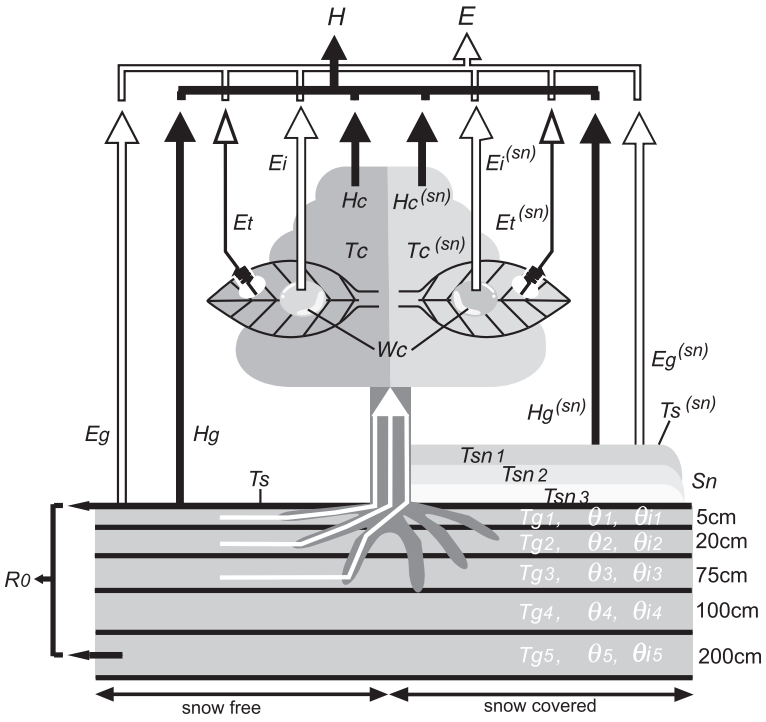

Fig. 1. Schematic diagram of the relation between the prognostic variables and the turbulent heat and vapor fluxes in MATSIRO. The symbols of the variables are listed in Tables 1 and 4. Black thick arrows denote sensible heat fluxes. White thick arrows denote evaporation, and white thin arrows denote transpiration.

paper, the structure of MATSIRO is summarized in Section 2, each component is described in Section 3, and a summary is provided in Section 4.

2. Structure of MATSIRO

2.1. General structure

The canopy is expressed with a single layer in MATSIRO. The energy balance is solved at the ground surface and the canopy surface separately, and the energy and water exchange between the ground surface and the atmosphere at a reference height and between the canopy surface and the atmosphere is estimated, respectively. The surface fluxes are calculated in the snow-free and snow-covered portions separately in a grid cell. The energy balance is thus solved at four surfaces in a grid cell. Namely, the ground surface and canopy surface temperatures, T_s and T_c, are determined in snow-free and snow-covered portions (Fig. 1). The calculated fluxes in the two portions are averaged by weighting with the fractions of the portions, to be used as the surface boundary condition of the atmosphere.

In solving the energy balance, the radiation, the sensible heat flux, the transpiration and the interception evaporation from canopy, the evaporation and the sublimation from the ground and snow surfaces, and the heat conduction into ground and snow are considered. The canopy water, w_c, is prognosticated from a balance equation of precipitation, interception evaporation, and dripping. The snow mass is prognosticated from snowfall, snowmelt, refreezing of rainfall and snowmelt, and sublimation. The number of snow layer is variable from one to three depending on the snow water equivalent (hereafter SWE), S_n. The snow albedo is prognosticated using the snow temperature, T_{sn}, and the effect of aging. Soil has five layers and those thicknesses are 5, 20, 75, 100, and 200 cm from the surface (Fig. 1). The soil temperature, T_g, the soil moisture, θ, and the frozen soil moisture, θ_i, are calculated in each layer of soil for the whole grid (i.e., not separated for snow-free and snow-covered portions).

The internal prognostic and diagnostic variables of MATSIRO are listed in Table 1. The external parameters are specified with the horizontal distributions, or in accordance with the land cover type or the soil type (Table 2). The values of the external parameters are determined after Sellers et al. (1996).

Table 1
Internal prognostic and diagnostic variables of MATSIRO

Variable	Description	Unit	Array[a]
Prognostic variables			
in LNDFLX[b]			
T_s	surface temperature	K	
T_c	canopy temperature	K	
in LNDSTP			
T_g	soil temperature	K	soil layer (5)
θ	soil moisture (solid + liquid)	m^3/m^3	soil layer (5)
θ_i	frozen soil moisture	m^3/m^3	soil layer (5)
w_c	canopy water	m^3/m^2	–
S_n	snow water equivalent	kg/m^2	–
T_{sn}	snow temperature	K	snow layer (1–3)
α_{sn}	snow albedo	–	V/N/I[c]
Diagnostic variables			
in LNDFLX[b]			
τ_x	zonal wind stress	N/m^2	–
τ_y	meridional wind stress	N/m^2	–
H	sensible heat flux	W/m^2	–
E_i	interception evaporation	$kg/m^2/s$	–
E_t	transpiration	$kg/m^2/s$	–
E_g	ground evaporation	$kg/m^2/s$	–
E_s	sublimation	$kg/m^2/s$	–
R_u	upward radiation	W/m^2	V/N/I[c]; D/R[d]
α_s	surface albedo	–	V/N/I[c]
F_g	surface heat conduction	W/m^2	–
ΔF	surface energy residual	W/m^2	–
in LNDSTP			
A_{Snc}	frozen fraction on canopy	–	–
F_{root}	root uptake	$kg/m^2/s$	soil layer (5)
R_o	runoff	$kg/m^2/s$	–

[a] Numeral in the parenthesis is the number of layers.
[b] Variables in LNDFLX are calculated for the snow-free and the snow-covered potions.
[c] V: visible, N: near infrared, and I: infrared.
[d] D: direct beam, R: diffuse radiation.

2.2. Calculation flow

MATSIRO consists of two parts; in one of which, the parameters are determined and the surface fluxes

Table 2
External parameters

Variable[a]	Description	Unit	Array[b]
Prescribed with horizontal distribution			
	land cover type	–	–
	soil type	–	–
LAI	leaf area index	m^2/m^2	monthly (12)
α_s	ground albedo	–	V/N[c]
β_s	surface mean slope	–	–
σ_z	standard deviation of altitude in a grid cell	m	–
Prescribed with land cover type			
	height of canopy top and bottom	m	–
r_f, t_f	leaf albedo and transmissivity	–	V/N[c]
	root distribution fraction	–	soil layer (5)
c_e, c_h, c_d	exchange coefficients of leaf (vapor, heat, and momentum)	–	–
	plant physiological parameters of Farquhar–Ball scheme	–	–
Prescribed with soil type			
c_g	soil heat capacity	$J/K/m^3$	soil layer (5)
k_g	soil heat conductivity	J/K/m/s	soil layer (5)
θ_s	porosity	m^3/m^3	soil layer (5)
K_s	saturation hydraulic conductivity	m/s	soil layer (5)
ψ_s	saturation hydraulic potential	m	soil layer (5)
B	exponent parameter of moisture retention curve	–	soil layer (5)

[a] Only the symbols appeared in the text are shown.
[b] Numeral in the parenthesis is the number of layers.
[c] V: visible and N: near infrared.

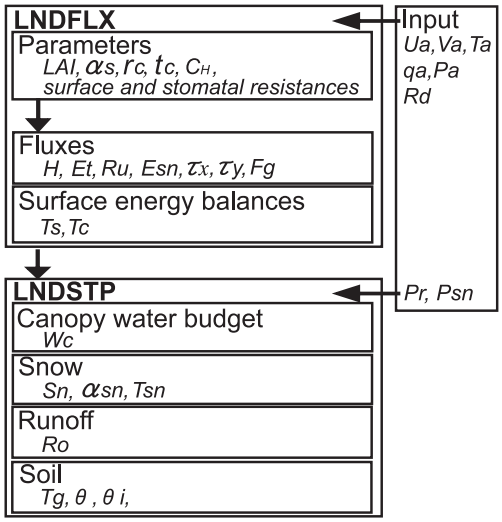

Fig. 2. Calculation flow of MATSIRO. The symbols of the variables are listed in Tables 1–3.

are calculated (LNDFLX), and in the other, the ground processes are treated (LNDSTP) (Fig. 2). The time steps of integration in LNDFLX and LNDSTP can be taken at different values independently, but both of them are taken at 60 min in the PILPS 2e experiment.

In LNDFLX, the external parameters (Table 2) and the input variables (Table 3) are set first, and then the albedo, the aerodynamic resistance, the surface evaporation resistance, and the stomatal resistance are evaluated from the schemes of radiative transfer in canopy, the turbulent transfer, and the photosynthesis. Then, the surface fluxes (the sensible and latent heat fluxes, the upward radiation, and the heat conduction into ground and snow) are diagnosed, and T_s and T_c are prognosticated, using the input variables (downward radiation, the atmospheric temperature and humidity, and so on), in the snow-free (F) and the snow-covered (S) portions. T_g and T_c are the so-called skin temperatures whose heat capacity is zero. The momentum flux is also calculated, though it is not fully explained here.

The downward radiation in the input data of Table 3 has six components: the direct insolation (D) and the diffuse radiation (R) in the three bands of wavelength,

Table 3
Input variables of MATSIRO

Variable	Description	Unit	Array
in LNDFLX			
U_a	zonal wind velocity	m/s	–
V_a	meridional wind velocity	m/s	–
T_a	atmospheric temperature	K	–
q_a	atmospheric humidity	kg/kg	–
P_a	atmospheric pressure	hPa	–
R_d	downward radiation	W/m^2	V/N/I[a], D/R[b]
cos ζ	cosine of solar zenith angle	–	–
in LNDSTP			
$P_{r,cum}$	convective rainfall	$kg/m^2/s$	–
$P_{r,ls}$	nonconvective rainfall	$kg/m^2/s$	–
$P_{sn,cum}$	convective snowfall	$kg/m^2/s$	–
$P_{sn,ls}$	nonconvective snowfall	$kg/m^2/s$	–

[a] V: visible, N: near infrared, and I: infrared.
[b] D: direct beam, R: diffuse radiation.

visible (V), near infrared (N), and infrared (I), indicated as D/R and V/N/I in the array column. In the offline simulation, the total solar radiation and the total long-wave radiation are usually given, so that the total solar radiation is divided into the visible and near-infrared bands in accordance with the cloudiness and the solar zenith angle (Goudriaan, 1977). The ratio of the direct insolation and the diffuse radiation is diagnosed from cloudiness (Goudriaan, 1977) for the visible and near-infrared bands, while all the downward long-wave radiation is taken as the diffuse radiation.

In LNDSTP, the canopy water budget, the snow, the runoff, and the soil temperature and moisture are calculated from the input variables (the convective and nonconvective rainfalls and snowfalls; Table 3) using the fluxes determined in LNDFLX as the upper boundary conditions (Fig. 2). The prognostic variables in LNDSTP are w_c calculated from the canopy water budget, SWE, T_{sn}, and the snow albedo, α_{sn}, calculated in the snow process, and the soil temperature and moisture calculated in the soil process. The runoff is diagnosed in the runoff scheme (Table 1). The detailed descriptions are presented in the following section.

3. Components of MATSIRO

3.1. Evaluation of parameters

The evaluation of the parameters mentioned in Section 2.2 is described in this section. The canopy top and bottom heights are specified associated with the land cover type (Table 2). The effective leaf area index (hereafter LAI) that is exposed to the atmosphere over snow cover is evaluated, assuming that the vertical distribution of leaves is uniform between canopy top and bottom. The snow depth is calculated from SWE with an assumption of a constant snow density (Section 3.5).

The albedo and transmissivity of canopy are calculated from an approximated solution of the radiative transfer in canopy (Watanabe and Ohtani, 1995), using the albedo and transmissivity of a leaf (r_f and t_f), the LAI, and the ground albedo. In this method, the analytic solution of the radiative transfer equation of shortwave in canopy is obtained assuming a random distribution of leaf angles. The leaf radiative parameters, r_f and t_f, are modified to be r'_f and t'_f with the presence of snow on canopy as

$$r'_f = \left(1 - \frac{w_c}{w_{cmax}}\right) r_f + \frac{w_c}{w_{cmax}} \alpha_{sn}, \quad (1)$$

$$t'_f = \left(1 - \frac{w_c}{w_{cmax}}\right) t_f + \frac{w_c}{w_{cmax}} t_{sn}, \quad (2)$$

where w_c is the canopy water (present as snow in this case), w_{cmax} is the canopy water capacity, and α_{sn} and t_{sn} are the snow albedo and transmissivity of a snow-covered leaf, respectively. t_{sn} is determined from α_{sn}.

The stomatal resistance is evaluated on the basis of a photosynthesis-stomatal resistance model (e.g., Farquhar et al., 1980; Ball, 1998; Collatz et al., 1990, 1991, 1992) after the scheme in SiB2 (Sellers et al., 1996). The soil moisture stress on photosynthesis is evaluated from the weighted mean of soil moisture with the root distribution fraction (Table 2). The resistance of ground surface evaporation, r_g, is calculated from the soil wetness in the uppermost layer as

$$r_g = a_1(1 - \theta_1/\theta_{s,1})/(a_2 + \theta_1/\theta_{s,1}), \quad (3)$$

which is functionally similar to Eq. (19) in Sellers et al. (1992), where θ_1 and $\theta_{s,1}$ are the volumetric soil moisture and the porosity in the uppermost layer, and a_1 and a_2 are the empirical coefficients at 800 and 0.2, respectively. The relative humidity at the ground surface, h_g, is used in the bulk formula of ground evaporation (see Eq. (4) and Table 4), which is calculated from the matric potential in the uppermost layer, ψ_1 (Philip, 1957).

The turbulent transfer coefficient is estimated by using the double-source model of Watanabe (1994), which is parameterized from a multilayer turbulent transfer model of canopy based on K-theory. In this scheme, the roughness length that represents the exchange considering both of the canopy heat/moisture source and the surface heat/moisture source (double-source) is estimated from the exchange coefficient of a leaf (c_h for heat, c_e for vapor, and c_d for momentum), LAI, canopy height, and the surface roughness length. Then the roughness is used in estimating the bulk transfer coefficient for the double-source (C_H for heat and C_E for moisture) based on

Table 4
List of turbulent fluxes

Type of surface	Fluxes		Parameters in the bulk formula					
	Definition symbol	Symbol	f	$\Re$	C	h	X_s	X_a
Snow-free canopy	sensible heat flux	H_c	$(1-A_{sn})$	ρc_p	$C_{Hc}v_a$	1	T_c	T_a
	interception evaporation	E_i	$(1-A_{sn})f_{wet}$	$L\rho$	$C_{Ei}v_a$	1	$q_{sat}(T_c)$	q_a
	transpiration	E_t	$(1-A_{sn})(1-f_{wet})$	$l_{evp}\rho$	$C_{Et}v_a$	1	$q_{sat}(T_c)$	q_a
Snow-free ground	sensible heat flux	H_g	$(1-A_{sn})$	ρc_p	$C_{Hg}v_a$	1	T_s	T_a
	evaporation	E_g	$(1-A_{sn})(1-f_{frz})$	$l_{evp}\rho$	$C_{Eg}v_a$	h_g	$q_{sat}(T_s)$	q_a
	sublimation	E_s	$(1-A_{sn})f_{frz}$	$l_{sub}\rho$	$C_{Eg}v_a$	h_g	$q_{sat}(T_s)$	q_a
Snow-covered canopy	sensible heat flux	$H_c^{(sn)}$	A_{sn}	ρc_p	$C_{Hc}^{(sn)}v_a$	1	$T_c^{(sn)}$	T_a
	interception evaporation	$E_i^{(sn)}$	$A_{sn}f_{wet}$	$L\rho$	$C_{Ei}^{(sn)}v_a$	1	$q_{sat}(T_c^{(sn)})$	q_a
	transpiration	$E_t^{(sn)}$	$A_{sn}(1-f_{wet})$	$l_{evp}\rho$	$C_{Et}^{(sn)}v_a$	1	$q_{sat}(T_c^{(sn)})$	q_a
Snow-covered ground	sensible heat flux	$H_g^{(sn)}$	A_{sn}	ρc_p	$C_{Hg}^{(sn)}v_a$	1	$T_s^{(sn)}$	T_a
	sublimation	$E_s^{(sn)}$	A_{sn}	$l_{sub}\rho$	$C_{Eg}^{(sn)}v_a$	1	$q_{sat}(T_s^{(sn)})$	q_a

A_{sn} is the snow-covered ratio, f_{wet} is the coverage of water on leaf, and f_{frz} is the frozen ratio in the uppermost soil layer. ρ is the density of the atmosphere, c_p is the specific heat of air at a constant pressure, l_{evp} and l_{sub} are the latent heat of evaporation and sublimation, respectively, L is equal to l_{sub} ($T_c<0$ °C) or l_{evp} ($T_c>0$ °C), C_{flux} are the bulk coefficients for the flux, v_a is the horizontal wind speed, and h_g is the relative humidity at the surface.

the Monin–Obukhov similarity theory. Assuming no exchange between a leaf and the canopy air, the roughness length and then the bulk transfer coefficients for the surface source only are estimated similarly (C_{Hg} for heat and C_{Eg} for moisture). The bulk transfer coefficients for the canopy source only (C_{Hc} for heat and C_{Et} (transpiration) and C_{Ei} (interception) for moisture) are estimated by the difference between the double-source bulk coefficient and the surface-source bulk coefficient (see Watanabe, 1994 for the details). In estimating the bulk transfer coefficient for transpiration, C_{Et}, the moisture exchange coefficient of a leaf, c_e, is modified first, using the stomatal resistance, r_c, in the following way, and then incorporated in the estimation of the roughness:

$$c_e = \frac{1}{1/c_h + r_c u_{CAS}}, \tag{4}$$

where u_{CAS} is the wind speed in canopy air space, which is simply assumed to be half of the wind speed at the canopy top that is diagnosed from the similarity theory. The ground surface resistance, r_g, is incorporated in the bulk transfer coefficient for evaporation, C_{Eg}, by modifying the surface roughness length at the ground, z_{Eg}, as

$$z_{Eg} = z_{Hg}\exp(-k_r u^* r_g), \tag{5}$$

where k_r is the von Karman constant and u^* is the friction velocity. z_{Hg} is the roughness length at the ground for sensible heat since the roughness for the unrestrained vapor transfer is assumed to be equal to that for sensible heat.

3.2. Surface fluxes

The surface fluxes and temperatures at the next time step are calculated simultaneously by solving the energy balance equations (Section 3.3) with an implicit scheme. The turbulent fluxes are written in the bulk formulae, whose general form is written as

$$\Im^{\tau+1} = f\Re C(hX_s^{\tau+1} - X_a), \tag{6}$$

where $\Im$ is a turbulent flux, f is the fractional coverage in a grid cell, $\Re$ is the physical constant, h is a coefficient, X_s is the surface condition, and X_a is the atmospheric condition. The superscript, $\tau+1$, denotes the next time step. The fluxes calculated at the four surfaces in a grid cell (Section 2.1) are listed in Table 4. The superscript (sn) denotes the snow-covered portion, whose ratio is A_{sn}. There are the sensible heat flux, the interception evaporation, and the transpiration at the canopy surface. The coverage of water on leaf, f_{wet}, is considered in calculating the interception evaporation and the transpiration. There are the sensible heat flux, the ground evaporation and sublimation at the ground surface. The frozen ratio in the uppermost soil layer, f_{frz}, is considered in calculating

the ground evaporation and the sublimation. The interception evaporation is taken as sublimation/evaporation when T_c (or $T_c^{(sn)}$ for the snow-covered portion) is below/above the freezing point.

The bulk coefficients for transpiration and ground evaporation, C_{Et} and C_{Eg}, are evaluated using the roughness that considers the stomatal and surface resistances, respectively (Section 3.1; Watanabe, 1994). Under the condition of dew formation (i.e., a downward vapor flux), however, the turbulent transfers from the atmosphere to the ground and canopy surfaces are not restrained by the stomatal and surface resistances. Then the bulk coefficients evaluated from the unrestrained roughness are used in this case. The unrestrained coefficient for vapor is the same as that for a sensible heat flux, C_{Hc}, since the aerodynamic coefficient for energy and vapor is assumed to be equal. The bulk coefficient for interception evaporation, C_{Ei}, is taken at the same value as C_{Hc} because of the same assumption.

The ground heat conduction fluxes in the snow-free and snow-covered portions are calculated by a heat conduction equation, using T_s and $T_s^{(sn)}$, and the uppermost soil and snow temperatures. The upward radiation is calculated using the albedo evaluated in Section 3.1.

3.3. Surface heat balance

The surface heat balances are solved by an implicit scheme at the ground and canopy surfaces in the snow-free and snow-covered portions to determine the ground surface and canopy temperatures (Section 2.1). The heat balances are written as

$$\Delta_c = H_c + R_c + E_i + E_t, \tag{7}$$

$$\Delta_g = H_g + R_g + E_g + E_s - F_g, \tag{8}$$

$$\Delta_c^{(sn)} = H_c^{(sn)} + R_c^{(sn)} + E_i^{(sn)} + E_t^{(sn)}, \tag{9}$$

$$\Delta_g^{(sn)} = H_g^{(sn)} + R_g^{(sn)} + E_s^{(sn)} - F_g^{(sn)}, \tag{10}$$

where Δ_c and Δ_g are the energy divergence, R_c and R_g are the net radiation, and F_g is the heat conduction to the ground. The superscript (sn) denotes the snow-covered portion similar to Table 4. Note that the divergent (i.e., outgoing) flux is taken as positive for R_c and R_g. The equations to calculate R_c and R_g are described in Appendix A. Since the heat capacity of canopy is assumed to be zero in MATSIRO, the heat conduction term does not appear in the canopy energy balance equations (Eqs. (7) and (9)). The canopy surface temperatures calculated from Eqs. (7) and (9) are taken as the canopy temperatures.

Two cases, the usual case (U) and the snowmelt case (M), are considered in solving the energy balance. In case U, Eqs. (7)–(10) are solved assuming Δ_c and Δ_g are zero, then T_s and T_c are updated. If T_s or T_c estimated in case U is higher than the freezing point and snow or ice exists, case M is applied. In case M, the surface temperature is fixed at the freezing point, and Δ_c and Δ_g are calculated from Eqs. (7)–(10). Then Δ_c and Δ_g are used for the latent heat of snowmelt (or ice melt) in LNDSTP (Section 3.5).

After the surface energy balance is numerically solved, the estimated surface temperatures and fluxes may be out of the physically acceptable range. The correction is applied in those cases, such as negative atmospheric specific humidity, negative soil moisture, negative canopy water, and negative SWE. After the fluxes are finalized, the transpiration is distributed among each soil layer in proportion to the root distribution fraction. In the last part of the surface heat balance, the phase of canopy water is diagnosed from the canopy temperature with the threshold of the freezing point.

3.4. Canopy water balance

The canopy water is calculated from a balance equation of the evaporation (or sublimation), the precipitation interception, and the dripping. The canopy water is divided into frozen and unfrozen water, $w_{c(w)}$ and $w_{c(i)}$, using the frozen ratio on canopy (Appendix B). The balance equations of $w_{c(w)}$ and $w_{c(i)}$ are calculated respectively as

$$\frac{dw_{c(w)}}{dt} = I_r - D_r - E_{i(w)}, \tag{11}$$

$$\frac{dw_{c(i)}}{dt} = I_{sn} - D_{sn} - E_{i(i)}, \tag{12}$$

where I_r and I_{sn} are the interceptions of rainfall and snowfall, D_r and D_{sn} are the dripping of water and

snow on canopy, and $E_{i(w)}$ and $E_{i(i)}$ denote the evaporation and sublimation parts of E_i.

It is indicated in the previous studies (e.g., Dolman and Gregory, 1992; Eltahir and Bras, 1993) that the subgrid scale distribution of rainfall and canopy water storage is important in calculating the interception evaporation at a coarse horizontal resolution, such as those used in climate studies. In MATSIRO, the convective precipitation is considered to occur in a part of a grid cell, though the subgrid heterogeneity of canopy water storage is ignored for simplicity. The interception is calculated separately for a portion where both the convective and nonconvective precipitation occur (stormy area), and for a portion where only the nonconvective precipitation occurs (calm area). I_r and I_{sn} are estimated as the sum of the interceptions in the two areas,

$$I_r = A_{cum} I_{r,cum} + (1 - A_{cum}) I_{r,ls}, \tag{13}$$

$$I_{sn} = A_{cum} I_{sn,cum} + (1 - A_{cum}) I_{sn,ls}, \tag{14}$$

where A_{cum} is the fraction of stormy area and the subscripts cum and ls denote the stormy and calm areas. A_{cum} is simply assumed to be a constant value 0.1 in this study. The four components of the interception ($I_{r,cum}$, $I_{r,ls}$, $I_{sn,cum}$, and $I_{sn,ls}$) are calculated as

$$I_{r,cum} = \min[f_{LAI}(P_{r,ls} + P_{r,cum}/A_{cum}), (w_{cmax} - w_{c(w)})/\Delta t], \tag{15}$$

$$I_{r,ls} = \min[f_{LAI} P_{r,ls}, (w_{cmax} - w_{c(w)})/\Delta t], \tag{16}$$

$$I_{sn,cum} = \min[f_{LAI}(P_{sn,ls} + P_{sn,cum}/A_{cum}), (w_{cmax} - w_{c(i)})/\Delta t], \tag{17}$$

$$I_{sn,ls} = \min[f_{LAI} P_{sn,ls}, (w_{cmax} - w_{c(i)})/\Delta t], \tag{18}$$

where min[a,b] means to take the smaller value between a and b, and f_{LAI} is the interception efficiency of LAI. f_{LAI} is equal to LAI when LAI is lower than unity, and equal to unity when LAI is higher than unity. Namely, all the precipitation is intercepted when LAI is higher than unity until w_c reaches w_{cmax}. The dripping is introduced after Rutter et al. (1975) as

$$D = D_1 \exp(D_2 w_c), \tag{19}$$

where D denotes D_r or D_{sn} in Eqs. (11) and (12), w_c denotes $w_{c(w)}$ or $w_{c(i)}$ in Eqs. (11) and (12), and D_1 and D_2 are the empirical constants 1.14×10^{-11} and 3.7×10^3, respectively.

3.5. Snow

The snow water equivalent (SWE), S_n, is prognosticated from a balance equation,

$$\frac{dS_n}{dt} = P^*_{sn} - E^{(sn)}_s - M_{sn} + F_R, \tag{20}$$

where P^*_{sn} is the snowfall affected by the canopy interception and dripping (Section 3.4), M_{sn} is the snowmelt, and F_R is the refreeze of snowmelt and the freeze of rainfall. The subgrid snow fraction, A_{sn}, is defined as

$$A_{sn} = \min\left[\sqrt{S_n/S_{nmax}}, 1\right], \tag{21}$$

where S_{nmax} is a critical value at which the whole of grid is covered with snow. S_{nmax} is one of the parameters for model calibration, and taken at 100 kg/m^2. It is confirmed that, with S_{nmax} being this value, the seasonal change in global snow cover in the global offline experiment using the same input data as in the Global Soil Wetness Project phase-I (Chen and Mitchell, 1999) is similar to that obtained by the satellite observation.

The number of snow layer is determined uniquely from S_n as shown in Fig. 3. The snow density is assumed to have a constant value, 300 kg/m^2, to calculate the thickness of the snow layer. The snow temperature, T_{sn}, is prognosticated by a thermal conduction equation,

$$c_i \frac{dT_{sn}}{dt} = \frac{\partial}{\partial z} k_{sn} \frac{\partial T_{sn}}{\partial z}, \tag{22}$$

where c_i is the snow heat capacity and k_{sn} is the snow thermal conductivity. The upper boundary conditions are $F^{(sn)}_g$ and $\Delta^{(sn)}_g$ in Eq. (10). At the lower boundary, the heat conduction is calculated between the lowest snow layer and the uppermost soil layer assuming no flux convergence between snow and soil. Then Eq. (22) is solved by a backward Euler scheme since it is the simplest scheme with which a diffusion equation can stably be solved. When T_{sn} is above the freezing point, the internal energy above the freezing point is

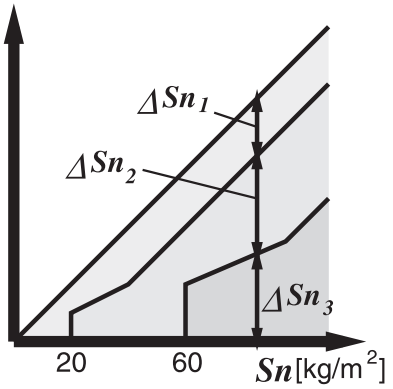

Fig. 3. The relation between snow water equivalent, S_n, and the snow layer.

used for the snowmelt, M_{sn}, and T_{sn} is set to the freezing point. Since the liquid water content in the snow layer is not considered, all of the snowmelt percolates to the layer below and refreezes there until the latent heat of freezing compensates for the internal energy below the freezing point. Then T_{sn} in the layer is adjusted for the latent heat of freezing. The rainfall also freezes in snow in a similar way to the snowmelt.

The snow albedo is changed in accordance with the time since the last snowfall and the snow temperature, considering the densification, the metamorphism, and the soilage of snow. It is prognosticated using an *aging* factor, A_g, after Wiscombe and Warren (1980) as

$$\alpha_b = \alpha_{b,new} - \frac{A_g}{1+A_g}(\alpha_{b,new} - \alpha_{b,old}), \tag{23}$$

where α is the snow albedo with the subscript b that denotes the radiation band (V/N/I; Section 2.2), $\alpha_{b,new}$ is the albedo of newly fallen snow for the band b, and $\alpha_{b,old}$ is the albedo of old snow for the band b. The snow albedo for visible and near-infrared bands are reduced with the passage of time since $\alpha_{b,old}$ is lower than $\alpha_{b,new}$, while that for infrared band is increased since $\alpha_{I,old}$ is higher than $\alpha_{I,new}$.

The snow albedo is refreshed by the snowfall at the refreshing rate, $\Delta\alpha_b$, calculated as

$$\Delta\alpha_b = \min\left[\frac{(P_{sn,cum} + P_{sn,ls})}{P_{sn,crt}}\Delta t, 1\right](\alpha_{b,new} - \alpha_b), \tag{24}$$

where $P_{sn,crt}$ is the critical snowfall amount at which the snow albedo is completely refreshed to $\alpha_{b,new}$.

3.6. Runoff

Four types of runoff are considered in MATSIRO: the base flow, the saturation excess runoff (Dunne runoff), the infiltration excess runoff (Horton runoff), and the overflow of the uppermost soil layer. To estimate the first three types, a simplified TOPMODEL (Beven and Kirkby, 1979) is applied. Though TOPMODEL usually requires a detailed elevation data over the domain of interest, it is difficult to treat such data at a global scale. Therefore, in MATSIRO, the subgrid topography in a grid cell is roughly approximated as repetition of a slope with a uniform slope angle of β_s and with the distance between ridge and valley of L_s (Fig. 4). The slope base length L_s is estimated by

$$L_s = 2\sqrt{3}\sigma_z/\tan\beta_s, \tag{25}$$

where σ_z is the standard deviation of subgrid topography in the grid box. When this simplified subgrid topography is applied to the TOPMODEL, the water table depth $z(x)$ at a point distant from the valley by a distance x is reduced to

$$z(x) = -\frac{1}{f}\ln\left(\frac{f_{atn}xR}{K_0\tan\beta_s}\right), \tag{26}$$

where f_{atn} is the reduction factor of hydraulic conductivity with soil depth, R is the recharge rate at the water

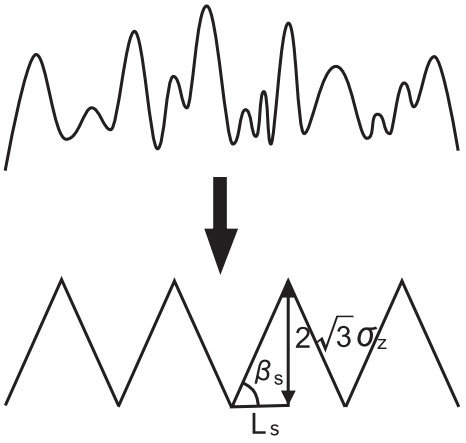

Fig. 4. Schematic diagram of the simplification of the subgrid topography used in the TOPMODEL of MATSIRO.

table, and K_0 is the saturation hydraulic conductivity at the surface. With a common assumption of TOPMODEL that R is horizontally uniform, $z(x)$ is written as

$$z(x) = \bar{z}_{\mathrm{WT}} - \frac{1}{f_{\mathrm{atn}}}\left(\ln\frac{x}{L_{\mathrm{s}}} + 1\right), \tag{27}$$

where $\bar{z}_{\mathrm{WT}}$ is the mean water table depth of the grid box. Stieglitz et al. (1997) proposed a probability density function (hereafter PDF) approach of the application of TOPMODEL to large-scale models. Our approach is equivalent to that of Stieglitz et al. (1997) with a uniform distribution applied to the PDF of topographic index.

The vertical distribution of soil moisture calculated by the Richards equation (Section 3.7) and the estimation of runoff by TOPMODEL are coupled in our scheme in a similar way to that in Stieglitz et al. (1997). The water table depth is diagnosed from the vertical distribution of soil moisture. This is used for the mean water table depth, $\bar{z}_{\mathrm{WT}}$, of the simplified TOPMODEL. A frozen table under the water table is also considered in calculating the base flow, if it is present. The calculated runoff is used in updating the vertical profile of soil moisture with the Richards equation (Section 3.7).

It is generally assumed in the TOPMODEL that the ground water flow at a point in the slope is equal to the accumulated ground water recharge in the upper area (i.e., a quasi-equilibrium assumption). Namely, the ground water flow is greater in the lower part of the slope. It is thus induced that the water table depth is shallower in the lower area, and, in some cases, the water table comes up to the surface to form the saturated area around a river channel. With our assumption of simplified subgrid topography, the saturation fraction, A_{sat}, is reduced to

$$A_{\mathrm{sat}} = 1 - \exp(f_{\mathrm{atn}}\bar{z}_{\mathrm{WT}} - 1), \tag{28}$$

and the base flow rate, R_{Ob}, which is equal to the recharge rate, R, with the quasi-equilibrium assumption of TOPMODEL, is reduced to

$$R_{\mathrm{Ob}} = R = \frac{K_0 \tan\beta_{\mathrm{s}}}{f_{\mathrm{atn}} L_{\mathrm{s}}} \exp(1 - f_{\mathrm{atn}}\bar{z}_{\mathrm{WT}}). \tag{29}$$

It is found in the PILPS 2e experiment that the ratio of the surface runoff to the base flow is sensitive to K_0, similarly to other LSMs with TOPMODEL (Niu, 2001, personal communication), though the total runoff is not sensitive so much to K_0.

The saturation excess runoff, R_{Os}, denotes the runoff caused by precipitation over the saturated area around the river channel; thereby, it is estimated as

$$R_{\mathrm{Os}} = f_{\mathrm{sat}} A_{\mathrm{sat}} (P^*_{\mathrm{r,cum}} + P^*_{\mathrm{r,ls}}), \tag{30}$$

where $P^*_{\mathrm{r,cum}}$ and $P^*_{\mathrm{r,ls}}$ are the precipitation affected by canopy in the stormy and calm areas (i.e., $P_{\mathrm{r,cum}} - I_{\mathrm{r,cum}} + D_{\mathrm{r,cum}}$ and $P_{\mathrm{r,ls}} - I_{\mathrm{r,ls}} + D_{\mathrm{r,ls}}$; see Section 3.4). f_{sat} is a calibration parameter to control the surface runoff, which corresponds to the river channel fraction in the saturated area. It would be equal to unity (i.e., all of $P^*_{\mathrm{r,cum}} + P^*_{\mathrm{r,ls}}$ in the saturated area becomes runoff), for example, in the mountainous area. In contrast, it is rather reasonable to assume that only a part of $P^*_{\mathrm{r,cum}} + P^*_{\mathrm{r,ls}}$ would immediately become runoff in a plain area in the high latitudes (e.g., low land of the experimental catchment of PILPS 2e) where it is usually wet and marshy. By taking a small value as 0.2 for f_{sat}, the overestimated surface runoff is reduced in the PILPS 2e experiment.

The infiltration excess runoff, R_{Oi}, is estimated as the sum of those in the stormy and calm areas, $R_{\mathrm{Oi,cum}}$ and $R_{\mathrm{Oi,ls}}$:

$$R_{\mathrm{Oi}} = A_{\mathrm{cum}} R_{\mathrm{Oi,cum}} + (1 - A_{\mathrm{cum}}) R_{\mathrm{Oi,ls}}, \tag{31}$$

$$R_{\mathrm{Oi,cum}} = (1 - A_{\mathrm{sat}})\max[P^*_{\mathrm{r,cum}}/A_{\mathrm{cum}} + P^*_{\mathrm{r,ls}} - K_{\mathrm{s},1}, 0], \tag{32}$$

$$R_{\mathrm{Oi,ls}} = (1 - A_{\mathrm{sat}})\max[P^*_{\mathrm{r,ls}} - K_{\mathrm{s},1}, 0], \tag{33}$$

where $\max[a,b]$ means to take the greater value between a and b, and $K_{\mathrm{s},1}$ is the saturation hydraulic conductivity in the uppermost layer. It is assumed that there is no correlation between the distribution of the saturation area and the stormy area in calculating R_{Os} and R_{Oi}.

The overflow of the uppermost layer, R_{Oo}, denotes the runoff induced by the oversaturation at the surface. In contrast to the three kinds of runoff described above, R_{Oo} is considered to occur over the entire grid. It is calculated as

$$R_{\mathrm{Oo}} = \frac{\rho_{\mathrm{w}} \Delta z_{\mathrm{g},1}}{\Delta t} \max[\theta_1 - \theta_{\mathrm{s}} - \theta_{\mathrm{str}}, 0], \tag{34}$$

where ρ_w is the water density, $\Delta z_{g,1}$ is the thickness of the uppermost soil layer, and θ_{str} is the surface water storage.

3.7. Soil

The soil temperature, T_g, is prognosticated by a thermal conduction equation,

$$C_g \frac{\partial T_g}{\partial t} = \frac{\partial F_g}{\partial z} = \frac{\partial}{\partial z} k_g \frac{\partial T_g}{\partial z}, \quad (35)$$

where F_g is the soil heat flux, C_g is the soil heat capacity, and k_g is the soil thermal conductivity. The upper boundary condition is the weighted average of the heat fluxes at the ground surface in the snow-free and the snow-covered portions of a grid cell, i.e., $(1-A_{sn})F_{g,1}+A_{sn}F_{sn,B}$, where $F_{sn,B}$ is the heat flux between snow and soil. The lower boundary condition is a zero heat flux. T_g in each layer is calculated using a backward Euler scheme, similarly to the snow temperature (Section 3.5). Then T_g is modified later for the latent heat of freeze and thaw.

The governing equation of unfrozen soil moisture, θ_w, is the Richards equation,

$$\frac{\partial \theta_w}{\partial t} = \frac{\partial F_w}{\partial z} + S_w, \quad (36)$$

where F_w is a soil moisture flux and S_w is a source/sink term, such as the root uptake and the runoff. Change in θ_w caused by freeze and thaw is considered later as a correction term. F_w is calculated from the vertical gradient of hydraulic potential, which is the sum of the matric potential, ψ, and the gravitational potential, as

$$F_w = K\left(\frac{\partial \psi}{\partial z} - 1\right), \quad (37)$$

where K is the hydraulic conductivity. K and ψ are calculated after the formula in Clapp and Hornberger (1979) with the modification for frozen soil as

$$K = f_K K_s \left(\frac{\theta_w}{\theta_s - \theta_i}\right)^{2B+3}, \quad (38)$$

$$\psi = \psi_s \left(\frac{\theta_w}{\theta_s - \theta_i}\right)^{-B}, \quad (39)$$

where f_K is the reduction factor for frozen soil, K_s is the saturation hydraulic conductivity, θ_i is the frozen soil moisture, B is the empirical parameter, and ψ_s is the saturation matric potential. K_s, ψ_s, and B are specified in accordance with the soil type (Table 2). f_K is defined after Smirnova et al. (2000) as

$$f_K = \left(1 - \frac{\theta_i}{\theta_w + \theta_i}\right)^a, \quad (40)$$

where a is unity. Eq. (36) is solved with a backward Euler scheme, similarly to the soil temperature, using Eqs. (37)–(40). It is confirmed that the reasonable solutions of T_g and θ_w are obtained with the uppermost layer being 5 cm and the time step being 1 hour in the PILPS experiment. The soil moisture flux may converge in the saturated zone below the water table due to the gravitational flow in calculating θ_w, and θ_w can become higher than the saturation. However, that oversaturation is not a real one, thus the oversaturated moisture is not treated as runoff but is corrected by putting it above the water table.

Soil freezing is calculated when the soil temperature calculated from Eq. (35) is below the freezing point and θ_w is higher than zero, and vice versa for soil thawing. The freeze/thaw amount, $\Delta\theta_i$, is diagnosed thermodynamically as

$$\Delta\theta_i = C_g(T_{mlt} - T_g)/\rho_w l_{mlt}, \quad (41)$$

where ρ_w is the water density and l_{mlt} is the latent heat of fusion. If $\Delta\theta_i$ is greater than θ_w (when freezing) or smaller than $-\theta_i$ (when thawing), $\Delta\theta_i$ is adjusted to the limit value. Then T_g, θ_w, and θ_i are modified to be consistent with $\Delta\theta_i$.

4. Summary and future plans

A detailed description of a land surface model, MATSIRO, is given. It is projected to be used for long-term simulations of climate studies. It is thus intended to represent all of the important processes on a physical basis as much as possible, but in a way as simple as possible. MATSIRO was validated both at the global scale (Takata, 2000) and at a local scale (Takata, 2001; Takayabu et al., 2001). It reproduced well the observed seasonal cycles of the energy and water balance.

It is well known that the snow albedo has strong impacts on the surface energy and water balances. Takayabu et al. (2001) stated that the surface energy and water balance is sensitive to the subgrid snow fraction. In MATSIRO, a simple relation between SWE and the subgrid snow fraction is assumed, using a critical value, S_{nmax} (Eq. (21)). SiB2 also uses a similar relation to evaluate the subgrid fraction (Sellers et al., 1996). However, in nature, the relation would depend on the subgrid topography. Moreover, the relation in accumulation would differ from that in ablation. Hence, a parameterization of the subgrid snow fraction needs to be developed by analyzing the high-resolution satellite snow cover data and the station data of snow, in order to represent the subgrid snow fraction in a realistic way. Besides, examinations on the sensitivity to the simple parameter, S_{nmax}, would be useful in improving the representation of the snow fraction.

In implementing the simplified TOPMODEL into MATSIRO, the probability density function of the topographic index in Stieglitz et al. (1997) is conceptually assumed to be uniform (Section 3.6). That is a tentative treatment, however. A more realistic form of the function should be used in a future LSM.

The surface storage parameter, θ_{str}, represents the water storage in subgrid lowlands. Since θ_{str} is averaged over a grid cell, it takes a small value when the grid size is large (e.g., AGCM). θ_{str} would be larger in the PILPS 2e experiment than in an AGCM experiment because the grid size is smaller. The same value of 1 mm as in the AGCM is used for this study, but θ_{str} should be calibrated in accordance with the horizontal resolution. Moreover, it should be parameterized from the subgrid topography in a future LSM to improve the reproducibility of the time sequence of runoff.

Acknowledgements

The authors gratefully acknowledge a lot of invaluable comments with the late lamented Dr. A. Numaguti from both the conceptual and technical points of view. Thanks are due to Dr. N. Saigusa for the valuable advice. Thanks are also due to the two anonymous reviewers for valuable comments that greatly help to improve the paper.

Appendix A. The net radiation at the ground and canopy surface

The net radiation divergence at the ground surface, $R_{\mathrm{g}}^{\mathrm{net}}$, is written as

$$R_{\mathrm{g}} = -(R_{\mathrm{SW}}^{\downarrow} - R_{\mathrm{SW}}^{\uparrow})\tau_{\mathrm{cSW}} - \varepsilon R_{\mathrm{LW}}^{\downarrow}\tau_{\mathrm{cLW}} + \varepsilon\sigma T_{\mathrm{s}}^{4} - \varepsilon\sigma T_{\mathrm{c}}^{4}(1-\tau_{\mathrm{cLW}}), \tag{A1}$$

where σ is the Stefan–Boltzman constant and

$$R_{\mathrm{SW}}^{\downarrow} = \sum_{b=V,N}\sum_{d=D,R} R_{(d,b)}^{\downarrow},$$

(downward shortwave radiation at the ground) (A2)

$$R_{\mathrm{SW}}^{\uparrow} = \sum_{b=V,N}\sum_{d=D,R} \alpha_{\mathrm{s}(d,b)} R_{(d,b)}^{\downarrow},$$

(upward shortwave radiation at the ground) (A3)

$$R_{\mathrm{LW}}^{\downarrow} = R_{(\mathrm{R,I})}^{\downarrow},$$

(downward longwave radiation at the ground) (A4)

$$\tau_{\mathrm{cSW}} = R_{\mathrm{SW}}^{\mathrm{gnd}}/(R_{\mathrm{SW}}^{\downarrow} - R_{\mathrm{SW}}^{\uparrow}),$$

(shortwave transmissivity of canopy) (A5)

$$\tau_{\mathrm{cLW}} = \exp(F \times \mathrm{LAI} \times d_{\mathrm{f}}),$$

(longwave transmissivity of canopy) (A6)

$$\varepsilon = 1 - \alpha_{\mathrm{s(r,I)}}, \qquad \text{(emissivity of ground surface)} \tag{A7}$$

where $R_{(d,b)}^{\downarrow}$ is the downward radiation at the surface of the beam d (D for direct and R for diffuse) and the radiation band b (V for visible, N for near infrared, and I for infrared), $\alpha_{\mathrm{s}(d,b)}$ is the ground surface albedo of the beam d and the radiation band b, and F and d_{f} are the constants at 0.5 and 1.66, respectively. $R_{\mathrm{SW}}^{\mathrm{gnd}}$ is calculated as

$$R_{\mathrm{SW}}^{\mathrm{gnd}} = \sum_{b=V,N}\sum_{d=d,r} \tau_{\mathrm{c}(d,b)} R_{(d,b)}^{\downarrow},$$

(shortwave radiation absorbed at the ground) (A8)

where $\tau_{c(d,b)}$ is the leaf transmissivity of the beam d and the radiation band b.

The net radiation at the canopy surface is written as

$$R_c = -(R^{\downarrow}_{SW} - R^{\uparrow}_{SW})(1 - \tau_{cSW}) - \varepsilon R^{\downarrow}_{LW}(1 - \tau_{cLW}) + (2\varepsilon\sigma T_c^4 - \varepsilon\sigma T_s^4)(1 - \tau_{cLW}). \quad (A9)$$

Appendix B. Diagnosis of the phase of canopy water

The phase of canopy water is diagnosed from the canopy temperature that is determined in the snow-free and snow-covered potions, T_c and $T_c^{(sn)}$. Then the frozen ratio on canopy, A_{Snc}, is defined as

$$A_{Snc} = A_{Sn} f_{Tc}(T_c^{(sn)}) + (1 - A_{sn}) f_{Tc}(T_c), \quad (B1)$$

where A_{Sn} is the subgrid snow fraction in a grid cell, $f_{Tc}(T)$ is the freezing factor that is equal to zero (unity) when temperature T is above (below) the freezing point, and the superscript (sn) denotes the snow-covered portion. A_{Snc} is used to calculate the canopy water balance since the water balance is solved for the entire grid. The canopy water, w_c, is divided into frozen and unfrozen water, $w_{c(w)}$ and $w_{c(i)}$, using A_{Snc} as

$$w_{c(w)} = (1 - A_{Snc}) w_c, \quad (B2)$$

$$w_{c(i)} = A_{Snc} w_c. \quad (B3)$$

References

Ball, J.T., 1998. An analysis of stomatal conductance. PhD thesis, Stanford University. 89 pp.

Beven, K.J., Kirkby, M.J., 1979. A physically based, variable contributing area model of basin hydrology. Hydrol. Sci. Bull. 24, 43–69.

Chen, F., Mitchell, K., 1999. Using the GEWEX/ISLSCP forcing data to simulate global soil moisture fields and hydrological cycle for 1987–1988. J. Meteorol. Soc. Jpn. 77, 167–182.

Clapp, R.B., Hornberger, G.M., 1979. Empirical equations for some soil hydraulic properties. Water Resour. Res. 14, 601–604.

Collatz, G.J., Berry, J.A., Farquhar, G.D., Pierce, J., 1990. The relationship between the Rubisco reaction mechanism and models of leaf photosynthesis. Plant Cell Environ. 13, 219–225.

Collatz, G.J., Ball, J.T., Grivet, C., Berry, J.A., 1991. Physiological and environmental regulation of stomatal conductance, photosynthesis and transpiration: a model that includes a laminar boundary layer. Agric. For. Meteorol. 54, 107–136.

Collatz, G.J., Ribas-Carbo, M., Berry, J.A., 1992. Coupled photosynthesis-stomatal conductance model for leaves of C_4 plants. Aust. J. Plant Physiol. 19, 519–538.

Dickinson, R.E., Shaikh, M., Bryant, R., Graumlich, L., 1998. Interactive canopies for a climate model. J. Climate 11, 2823–2836.

Dolman, J., Gregory, D., 1992. The parameterization of rainfall interception in GCMs. Q. J. R. Meteorol. Soc. 118, 455–467.

Eltahir, E.A.B., Bras, R.L., 1993. A description of rainfall interception over large areas. J. Climate 6, 1002–1008.

Famiglietti, J.S., Wood, E.F., 1994. Multiscale modeling of spatially variable water and energy balance processes. Water Resour. Res. 30, 3061–3078.

Farquhar, G.D., von Caimmerer, S., Berry, J.A., 1980. A biochemical model of photosynthetic CO_2 fixation in leaves of C_3 species. Planta 149, 78–90.

Goudriaan, J., 1977. Crop micrometeorology: a simulation study. Simulation Monographs. PUDOC, Wageningen. 257 pp.

Koster, R.D., Suarez, M.J., Ducharne, A., Stieglitz, M., Kumar, P., 2000. A catchment-based approach to modeling land surface processes in a general circulation model 1. Model structure. J. Geophys. Res. 105, 24809–24822.

Numaguti, A., Takahashi, M., Nakajima, T., Sumi, A., 1997. Description of CCSR/NIES Atmospheric General Circulation Model. CGER's Supercomputer Monograph Report, 3, NIES, Tsukuba, Japan, pp. 1–48.

Philip, J.R., 1957. Evaporation, and moisture and heat fields in the soil. J. Meteorol. 14, 354–366.

Rutter, A.J., Morton, A.J., Robins, P.C., 1975. A predictive model of rainfall interception in forests II. Generalization of the model and comparison with observations in some coniferous and hardwood stands. J. Appl. Ecol. 12, 367–380.

Sellers, P.J., Heiserr, M.D., Hall, F.G., 1992. Relations between surface conductance and spectral vegetation indices at intermediate (100 m^2 to 15 km^2) length scales. J. Geophys. Res. 97, 19,033–19,059.

Sellers, P.J., Randall, D.A., Collatz, G.J., Berry, J.A., Field, C.B., Dazlich, D.A., Zhang, C., Collelo, G.D., Bounoua, L., 1996. A revised land surface parameterization (SiB2) for atmospheric GCMs. Part I: model formulation. J. Climate 9, 676–705.

Smirnova, T.G., Brown, J.M., Benjamin, S.G., Kim, D., 2000. Parameterization of cold-season processes in the MAPS land-surface scheme. J. Geophys. Res. 105, 4077–4086.

Stieglitz, M., Rind, D., Famiglietti, J., Rosenzweig, C., 1997. An efficient approach to modeling the topographic control of surface hydrology for regional and global climate modeling. J. Climate 10, 118–137.

Takata, K., 2000. Sensitivity study on snowmelt discharge of Lena using a land surface model, "MATSIRO". Activity Report of GAME-Siberia, 1999, GAME Publication, No. 21, Nagoya Univ., Nagoya, Japan, pp. 73–76.

Takata, K., 2001. Estimation of summer heat and water fluxes at Tiksi using a one-dimensional land surface model. Activity Report of GAME-Siberia, 2000, GAME Publication, No. 26, Nagoya Univ., Nagoya, Japan, pp. 207–208.

Takata, K., Emori, S., 1999. Development and validation of a land surface model, "MATSIRO". Activity Report of GAME-Siberia, 1998, GAME Publication, No. 14, Nagoya Univ., Nagoya, Japan, pp. 103–106.

Takayabu, I., Takata, K., Yamazaki, T., Ueno, K., Yabuki, H., Haginoya, S., 2001. Comparison of the snow accumulation and the soil freezing processes among four land surface process models by using GAME/Tibet POP 97 data. J. Meteorol. Soc. Jpn. 79, 535–554.

Warrach, K., Stieglitz, M., Mengelkamp, H.-T., Raschke, E., 2002. Advantages of a topographically controlled runoff simulation in a soil–vegetation–atmosphere transfer model. J. Hydrometeorol. 3, 131–148.

Watanabe, T., 1994. Bulk parameterization for a vegetated surface and its application to a simulation of nocturnal drainage flow. Boundary-Layer Meteorol. 70, 13–35.

Watanabe, T., Ohtani, Y., 1995. A simple model of shortwave-radiation transport within canopy. J. Agric. Meteorol. 51, 57–60 (in Japanese).

Wiscombe, W.J., Warren, S.G., 1980. A model for the spectral albedo of snow: I. Pure snow. J. Atmos. Sci. 37, 2712–2733.